https://doi.org/10.5194/tc-2021-349
Preprint. Discussion started: 18 November 2021

The Cryosphere Discussions

Radiative penetration dominates the thermal regime and energetics of a shallow ice-covered lake in an arid climate

Wenfeng Huang[1,2]*, Wen Zhao[1], Cheng Zhang[1], Matti Leppäranta[3], Zhijun Li[4]*, Rui Li[1], Zhanjun Lin[2]

1 Key Laboratory of Subsurface Hydrology and Ecological Effects in Arid Region (the Ministry of Education), Chang'an University, Xi'an, China

2 State Key Laboratory of Frozen Soil Engineering, Northwest Institute of Eco-Environment and Resources, Chinese Academy of Science, Lanzhou, China

3 Institute of Atmospheric and Earth Sciences, University of Helsinki, Helsinki, Finland.

4 State Key Laboratory of Coastal and Offshore Engineering, Dalian University of Technology, Dalian, China

*Correspondence to: Wenfeng Huang (huangwenfeng@chd.edu.cn) and Zhijun Li (lizhijun@dlut.edu.cn)

Abstract. The Central Asia is characterized by cold and arid winter with very little precipitation (snow), strong solar insolation, and dry air. But little is known about the thermal regimes of ice and ice-covered lakes and their response to the distinct meteorology and climate in this region. In a typical large shallow lake, ice/snow processes and under-ice thermodynamics were observed for four winters between 2015 and 2019. Heat budgets at the ice-water interface and within the water column were investigated. Results reveal that persistent bare ice permits 20%–35% of incident solar radiation to transmit into the under-ice water, providing background source for under-ice energy flows and causing/maintaining high water temperature (up to 6–8°C) and high water-to-ice heat flux (annually mean 20–45 W m^{-2}) in mid-winter. Heat balancing indicates that the transmitted radiation and water-to-ice heat flux are the dominators and highly correlated. Both bulk water temperature and its structure respond sensibly to solar transmittance and occasional snow events. Complicated evolution of thermal structure was observed and under-ice convective mixing does not necessarily occur because of the joint governance of strong irradiance, sediment heating and salinity profile. Especially, salt exclusion of freezing changes both the bulk salinity and its structure, which plays a more important role in stability/mixing of the water column in the shallow lake.

1 Introduction

Lakes are important water resources and provide vital habitats for aquatic ecosystems. More than 55% of world lakes are located between 40 and 80°N in the north hemisphere (Verpoorter et al., 2014), and have potential to freeze seasonally (Kirillin et al., 2012), especially in Arctic, boreal, and temperate climate and high mountain regions. Due to distinct properties of ice compared to water, seasonal formation and decay of ice cover have tremendous impacts on lake water quality (Yang et al., 2016), physical and chemical conditions (Yang et al., 2021; Cavaliere and Baulch, 2018; Huang et al., 2019a),

https://doi.org/10.5194/tc-2021-349
Preprint. Discussion started: 18 November 2021

aquatic ecosystem (Griffiths et al., 2017; Song et al., 2019), and land-atmosphere mass and heat interaction (Wang et al., 2015; Franz et al., 2018). Therefore, common concerns have been widely reached on mapping the lake ice physics and its underlying physical mechanisms.

Field and modeling investigations on lake ice processes have a long history in northern temperate and boreal regions, such as Fennoscandia, central Europe, northern Canada, and the Great Lakes. Ice duration shortening has been documented currently in these lakes (Bernhardt et al., 2012; Lei et al., 2012; Karetnikov et al., 2017; Ptak et al., 2020). However, the lake ice regime in arid climate remains less studied due to lack of long-term observational record, such as in central Asia and high mountain regions, which are subject to quite different landscape, regional climate, and hydrological cycles compared with the northern temperate, boreal, and Arctic environment.

Lake thermal stratification dynamics is of great importance to hydrodynamics and transport of nutrients, oxygen and phytoplankton, which influence the limnological habitats and ecosystems. In freezing lakes, stable inversed thermal stratification usually forms and persists under the ice cover with the temperature typically smaller than the maximum density temperature (e.g. 3.98°C for freshwater). After the onset of melting, strong solar irradiance can penetrate the apparent ice cover into the water and drive turbulent convection (Bouffard et al., 2019; Volkov et al., 2019) until the bulk temperature reaches or surpasses the maximum density temperature or the breakup (Yang et al., 2020). However, in some shallow mid-latitude lakes, this is not the story. During melting, a warm middle layer can form and separate the overlying inversed thermal stratification and the underlying positive thermal stratification. Its temperature can grow up to around 10°C before the breakup (e.g. Huang et al., 2019b; Kirillin et al., 2021). This underlines the uniqueness of seasonally ice-covered lakes in mid-latitude arid regions and the importance of their different climates. It remains unclear how this stratification forms and evolves and how it interacts with the snow/ice processes.

After freeze-up, the ice cover shelters the lake from atmospheric forcing and deposits. The lake boundary is constituted by only the ice cover on the top and sediment at the bottom. The heat budget is governed by heat and radiation fluxes across the ice-water-sediment interfaces (Leppäranta, et al., 2019). But these fluxes, including solar radiation transmission, ice-water heat exchange and sediment heat release, have not been well quantified in mid-latitude arid region lakes. Especially, the ice-water heat flux, a key factor affecting the mass and energy balance of both ice and water, has been demonstrated to be remarkably higher in some central Asia lakes than those in Arctic and boreal lakes (Malm et al., 1997; Jakkila et al., 2009; Huang et al., 2019a,b; Lu et al., 2020). But the regime underpinning its high values is still unknown.

Lake Ulansuhai, a large shallow lake in the south border of Mongolia Plateau, is located in a typical central Asian arid climate zone and is covered by ice for 4–5 months annually. We performed 4-winter observations of snow/ice processes, solar radiation transfer and temperature profiles of air-ice-water-sediment column. Below, observations and models were combined 1) to reveal the seasonal and diurnal dynamic of lake temperature stratification under the ice in mid-latitude arid climate and 2) to quantify and balance the involved heat fluxes that determine the thermal state.

2 Methods

2.1 Study site

The Hetao Basin (ca. 6,000 km^2, mean altitude > 1,000 m), one of the oldest and largest irrigation area in China, is located in the central southern Mongolian Plateau that is controlled by a temperate

https://doi.org/10.5194/tc-2021-349
Preprint. Discussion started: 18 November 2021

continental climate. In the Hetao Basin, the annual sunshine duration is about 3,000–3,200 h, the annual air temperature is 5.6–7.4°C with the lowest and highest month temperature of –14– –11°C (Jan) and 22–24°C (Jul), the frost-free period is 130–150 d, and the annual precipitation is 150–400 mm and is concentrated in warm seasons. Most parts of the basin have been desertified or semi-desertified in recent decades.

Lake Ulansuhai (40°36′–41°03′N, 108°41′–108°57′E, altitude 1,019 m), a typical large shallow lake in desert/semi-desert region with a total area of about 306 km^2 (Fig. 1). It is a very important part of the irrigation and drainage system of the Hetao Basin, and its major water source comes from the farmland irrigation drainage and domestic sewage. The maximum and mean depth is 2.5–3.0 m and 1.0–1.5 m, respectively. The annual air temperature, hours of sunshine, precipitation, evaporation, wind speed, frost-free period is 7.3°C, 3,185 h, 224 mm, 1,502 mm, 3.5 m s^{-1}, and 152 d, respectively (Sun et al., 2011). The solar noon and altitude in winter is about 12:45±15 min and 41±10°, respectively. The ice cover is usually free of snow or only sparsely snow covered due to occasional snow events and strong winds.

The lake level is regulated through pumping water from the Yellow River via the main inflow canal in the western border. The total annual water supply is approximately 4 × 10^8 m^3, equivalent to the lake volume. But, in winter (Nov–Mar), very little surface inflow/outflow exists except some possible wastewater inflow (Sun et al., 2013), and the subsurface inflow is also negligible (Zhu et al., 2014). For more detailed information, please refer to Lu et al. (2020) and references therein.

According to our sampling tests in winter 2017, the lake water is weakly saline with salinity of 1.0–1.5 PSU before the ice-on and gradually increased to 2.5–3.0 PSU when the ice cover grows to its annual maximum due to freezing exclusion of salt.

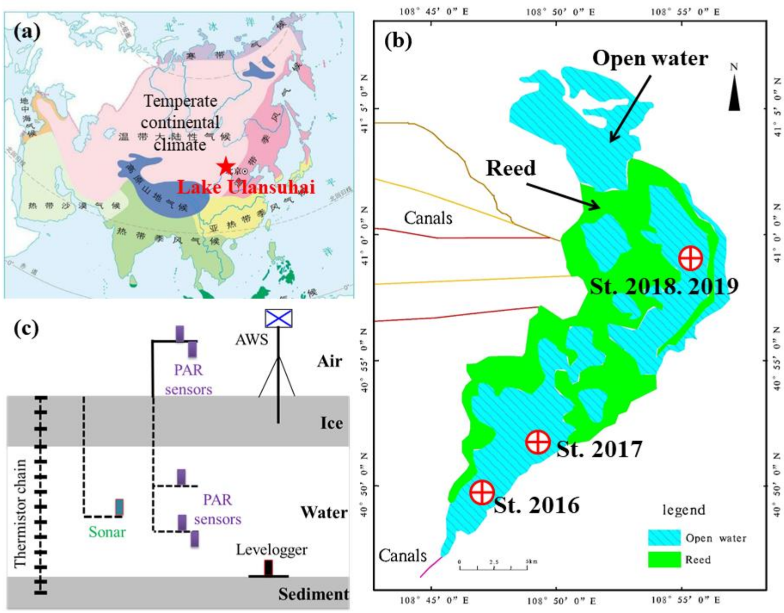

Figure 1. Locations of Lake Ulansuhai (a) and study sites (b) and the field instrumentation (c).

2.2 Data acquisition

During winters of 2015-2019, field campaigns were conducted in open water areas of Lake Ulansuhai (Fig. 1c). In each winter, an automatic weather station (AWS) was established on the ice cover, observing wind speed and direction, air temperature and humidity, total incident and reflected radiation (300–3000 nm), and the skin temperature of the ice/snow surface. An under-ice uplooking sonar (WUUL-1/2, Wuhan University, China) was used to measure the ice thickness evolution with accuracy of 2 mm. The snow thickness was measured manually using a snowstake every 1–2 days. The temperature profile of the air-ice-water-sediment column was observed using a thermistor chain (PTWD, Jinzhou Sunshine Technology Co. Ltd, China) at 5–10 cm spacing with accuracy of 0.05°C. TriOS spectral radiometers with accuracy of 0.04–0.06 mW m^{-2} nm^{-1} (RAMSES-ACC-VIS, TriOS, Germany) were used to measure the incident and reflected photosynthesis active radiation (PAR) over the ice/snow surface and under-ice downward irradiance. The water level change was measured using a temperature-pressure logger with accuracy of 0.05% (LTC Levelogger, Solinst, Canada) placed 20 cm above the sediment surface. All the above variables were recorded every 10 min. Information of all acquired datasets was summarized in Table 1 (also refer to Huang et al. (2021)).

Table 1. Data series acquired during four winter observations

Winter	2016	2017	2018	2019
Available duration	Jan 11–Mar 9	Jan 21–Mar 11	Jan 9–Feb 25	Jan 20–Feb 27
Water depth	220 cm	170 cm	143 cm	140 cm
Ice/snow thickness	√	√	√	√
Air-ice-water-sediment temperature	√ (21)	√ (24)	√ (27)	√ (17)
Under-ice irradiation	√ (1)	√ (2)	√ (3)	√ (2)
Under-ice upwelling radiation		√ (1)	√ (1)	
Water level		√		
Electric Conductivity		√ (3)		

Note: The observed variables were ticked with the total number of measuring depths showed in the brackets.

2.3 Data processing

In freshwater lakes the water temperature is much colder than 3.98°C with a weak inverse thermal stratification during freezing (Winter I phase), and typically a convective mixing layer forms between the top cold interfacial layer and the warm quiescent layer during melting (Winter II phase) (Kirillin et al., 2012). The stratification structure in Lake Ulansuhai was checked using temperature gradient following Kirillin et al. (2018).

After freeze-up, as illustrated in Fig. 2, thermal regime of the water column is governed by the solar irradiance penetrating through the ice cover (R_w), solar radiation absorbed by the lake sediment (if any) (R_{sed}), heat fluxes through ice-water (F_w) and water-sediment (F_{sed}) interfaces, and horizontal heat gain (F_h) from the neighboring water body. If the zero reference level for heat is defined as the heat content of liquid fresh water at its freezing point temperature, the heat content is $\rho_w c_w T_w h_w$ for water. The heat budget of water column is

$$R_w - R_{sed} + F_{sed} + F_h - F_w = \rho_w c_w h_w \frac{dT_w}{dt} + \rho_w c_w T_w \frac{dh_w}{dt}, \quad (1)$$

where ρ_w, c_w, and T_w is the density, specific heat capacity, and temperature of water, respectively. Other variables are defined in Fig. 2. The lateral heat transport F_h is negligible in this shallow lake with a flat

https://doi.org/10.5194/tc-2021-349
Preprint. Discussion started: 18 November 2021

The Cryosphere Discussions
Open Access
EGU

bottom (Rizk et al., 2014; Kirillin et al., 2015). The two terms on the right-hand side are the heat content changes induced by changes in the water temperature and level, respectively. The water level logger result indicated that the lake lost water through seepage to soil quite slowly (about 0.6 mm/d) during ice seasons, and the heat loss due to the bottom water seepage was estimated to be smaller than 0.8 W m^{-2} and thus was ignored compared to other heat fluxes.

Under-ice solar irradiance The light extinction coefficient of the under-ice water column was measured to be 2.1 m^{-1} under clear sky on Jan 7, 2018. Using the observed irradiance by under-ice spectral sensors, the solar irradiance at the ice-water interface (R_w) was derived from a one-band exponential decay law of light transfer in water column, following

$$R_w = R_d \exp(\kappa_w (z_d - h_i)), \quad (2)$$

where R_d is the observed downward irradiance at depth z_d, h_i is the ice thickness, and κ_w is the light extinction coefficient of water.

Sediment heat flux The effective thermal conductivity of the top sediment was estimated to be 0.2–0.7 W m^{-1}°C^{-1} using an optimal control model (Shi et al., 2014) based on the observed temperature profile of sediment. The heat exchange flux through the water-sediment interface (F_{sed}) was calculated from a gradient method,

$$F_{sed} = -\kappa_{sed} \left. \frac{\partial T_{sed}}{\partial z} \right|_{bottom} \approx -\kappa_{sed} \frac{\Delta T_{sed}}{\Delta z}, \quad (3)$$

where κ_{sed} is the thermal conductivity of sediment (= 0.5 W m^{-1}°C^{-1}) and T_{sed} is the observed sediment temperature.

Water-to-ice heat flux The water-to-ice heat flux can be derived from the heat balance at the ice-water interface,

$$F_w = Q_c - Q_l = -\kappa_i \left. \frac{\partial T_i}{\partial z} \right|_{z=h_i} - \rho_i L_f \frac{\partial h_i}{\partial t}, \quad (3)$$

Where Q_c and Q_l is the conductive heat within bottom ice and latent heat due to ice freezing/melting, ρ_i and L_f is the density and latent heat of fusion of ice, respectively. The first term on the right-hand side denotes the heat release/absorption due to ice freezing/melting, which can be derived from the ice thickness observation. The second term denotes heat conduction into the ice interior, which can be derived using the temperature gradient observed in the bottom ice layer.

The heat content change (i.e. the first term on the right-hand side of Eq. (1)) was calculated using the observed water temperature profiles.

Direct use of semi-hourly observed datasets brought high-frequency fluctuations in heat flux estimation. So, daily means of these fluxes were used for further analysis on seasonal dynamics.

https://doi.org/10.5194/tc-2021-349
Preprint. Discussion started: 18 November 2021

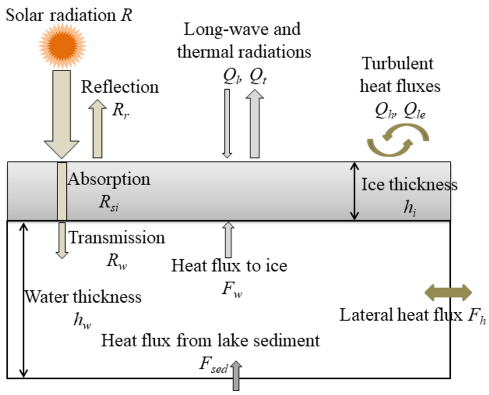

Figure 2. Heat budget components of the water column under the ice

2.4 Potential errors in heat flux estimation

Potential errors in the above heat flux estimation usually come from the measure accuracy of deployed apparatuses. We classified errors into four ranges: (a) negligible, less than 0.2 W m^{-2}, (b) minor, 0.2–1.0 W m^{-2}, (c) moderate, 1.0–2.0 W m^{-2}, and (d) crucial, greater than 2.0 W m^{-2} (Table 2). The thermistor accuracy is expected to influence F_s and F_{Tw} moderately, and the ice density influences the F_w moderately. Other heat fluxes suffer only to negligible or minor uncertainties induced by individual source. Errors from several sources may accumulate especially in F_w, but the accumulated errors in F_w should be less than 8%.

Table 2. Uncertainties in calculation of heat fluxes

Error source	Heat flux (W m^{-2})*			
	R_w	F_{sed}	F_w	$F_{Tw}=\rho_w c_w h_w \frac{dT_w}{dt}$
Radiation precision	N(0.08)	–	–	–
Thermistor precision	–	S(0.25)	M(1.1)	M(1.7)
Ice thickness	N(0.1)	–	–	N(0.01)
Ice growth rate	–	–	S(0.3)	–
Ice density	–	–	M(1.25)	–
Water density	–	–	–	N(0.2)

*Here N, S, M, and C denote negligible, minor, moderate, and crucial. Dashes (–) indicate inapplicable.

3 Results

3.1 Lake ice and temperature

Our observations were conducted during mid-winters covering the turning point from freezing to melting. The air temperature was consistently lower than 0°C, but its daily amplitude was very high (~10–16°C) and the peak at noon/afternoon could be close to 0°C (Fig. 3). Wind speed was generally lower than 4 m s^{-1} except occasional wind gusts that lead to snow or dust drifting. The relative humidity of air 2-m above the ice surface also showed evident diurnal cycle between 40% and 80%.

https://doi.org/10.5194/tc-2021-349
Preprint. Discussion started: 18 November 2021

The peak incident solar radiation each day was roughly 500–800 W m^{-2}, and its daily average was 80–200 W m^{-2} and showed a trend of increase from the beginning to the end of our observation. But the daily average was always smaller than 100 W m^{-2} due to prevailed cloudy or overcast skies in winter 2019. Occasional snowfalls usually brought about thin snow layers (< 6 cm) that continuously ablated due to wind blowing and thermal melting/evaporation. New snow covers could increase the surface albedo up to over 0.80 but this increment gradually disappeared within one week following the snowfall.

The ice thickness differed annually between 35 cm and 60 cm, accounting for 30%–60% of the mean lake depth. The bulk water temperature under the ice cover was 3–7°C and showed obvious diurnal cycles and synoptic decreased following snow events, evidencing the effect of transmitted solar radiation. The surface sediment was always warmer than the water column during the observation, indicating the sediment works as a heat source to warm the overlying water.

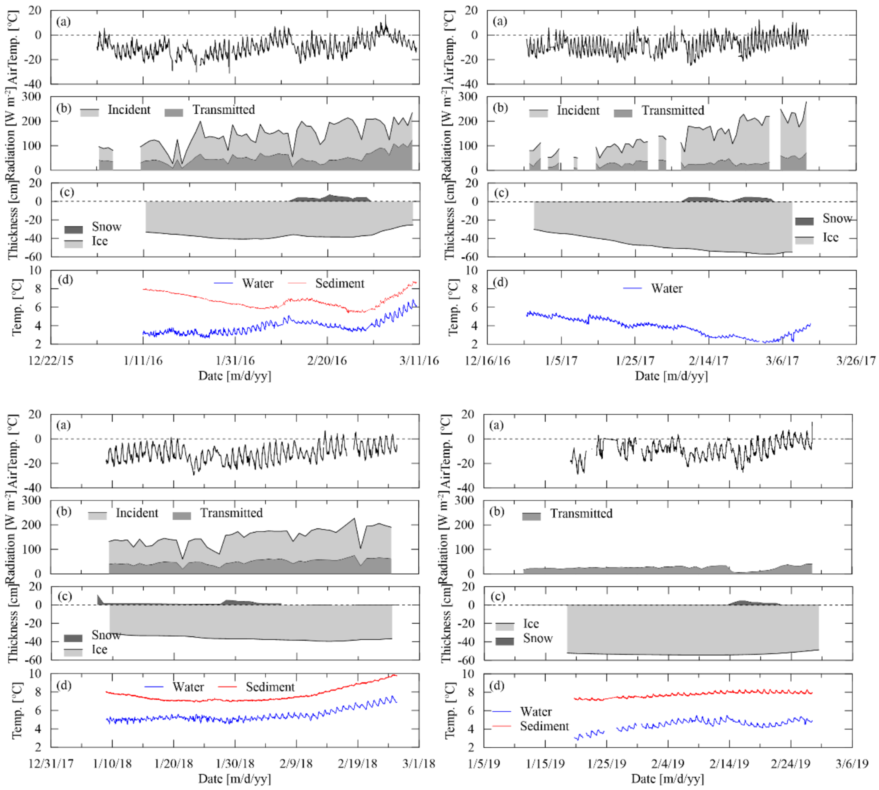

Figure 3. Observational air temperature *Ta* (a), daily means of incident and reflected solar radiation (b), snow and ice thickness (c), temperature of water column and surface sediment. (top left: winter 2016; top right: winter 2017; bottom left: winter 2018; bottom right: winter 2019)

3.2 Thermal stratification and mixing in midwinter

In mid-winters, the lake sediment was still very warm with surface temperature > 6°C, usually causing inverse temperature profile in water column (Fig. 4). Although our observations didn't cover the whole

https://doi.org/10.5194/tc-2021-349
Preprint. Discussion started: 18 November 2021

ice season, evident seasonal and annual variations were observed.

A common thin layer (10–30 cm) of strong inverse stratification (i.e. interface layer) prevailed just beneath the ice due to the large difference in temperature of the ice base (i.e. constantly at the freezing point) and the bulk water column, e.g. in winters 2016, 2018 and 2019. But in winter 2017, this thin top layer did not show up during our observational period and a persist thick inverse structure developed through the water column (Fig. 4b). Underneath the top cold interface layer, the temperature increased slowly downward to the warmer sediment (weak inverse structure) in winter 2019 and prior to 3 Mar in winter 2016 (Fig. 4a and 4d). After 3 Mar in winter 2016 and 10 Feb in winter 2018, a thermally homogeneous convective layer quickly developed after the bulk water temperature rose above approximately 7°C (Fig. 4a and 4c). Strikingly, before the formation of convective mixing in winter 2018, a "warm" zone of 30 cm (local maximum temperature) with temperature decreasing both downwardly and upwardly persisted at ~30 cm beneath the ice base.

Occasional snowfall events usually led to quick bulk cooling along the entire water temperature profile due to high reflection of new snow despite of their small thickness. The sensitive response of water temperature to snow events (actually changes in penetrated radiation) implies large heat flux from water to ice and the dominance of solar radiation in this lake.

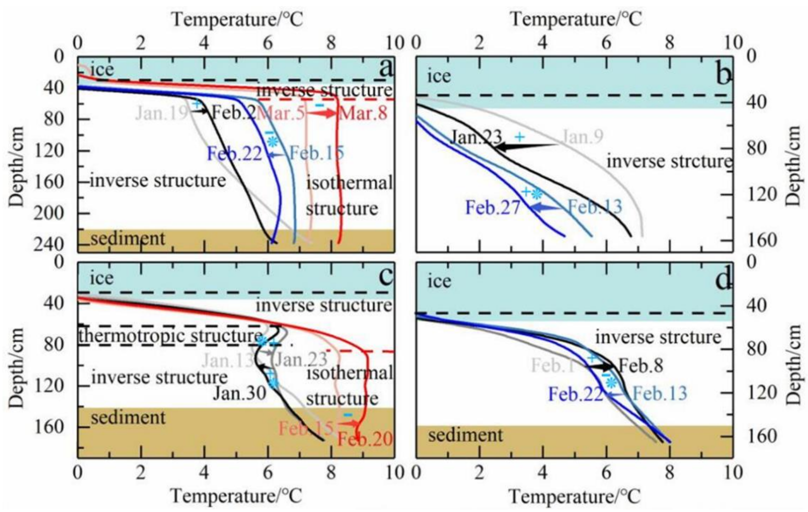

Figure 4. Daily profile evolution of water column during ice season of winters (a) 2016, (b) 2017, (c) 2018, and (d) 2019. Light blue and brown zones denote ice cover and bottom sediment, respectively. Blue stars (*) denote snowfalls and snow-covered periods. Plus (+) and minus (-) denote growth and melt stage of the ice cover.

Unconventionally, under-ice convection did not take place in all winters (only two of our four observational winters) and seems to develop just when the bulk water temperature goes up to 7°C. This temperature threshold is higher than the temperature of maximum density of freshwater (3.98°C) and saline water (<3.98°C). These annually-variable convections are believed to form conditionally and lake-specifically with proper water-sediment temperature and salinity profile. Water sampling indicated that, in this very shallow lake, the salt amount increases and structure changed simultaneously as the ice grew (Fig. 5). At the ice-on, the salinity showed a stable profile (increasing downwardly) and its

https://doi.org/10.5194/tc-2021-349
Preprint. Discussion started: 18 November 2021

impact on water density outweighed the impact of concurrent temperature gradient (i.e. on Jan 5). With the following ice growth, the bulk salinity increased but the salinity gradient decreased and the temperature gradient decreased. Consequently, the weakened salinity gradient could persistently outweigh or offset the impact of temperature profile on water density through the growing period (before Mar 4). When the ice started melting, the salinity gradient turned larger due to fresh meltwater release from the top, the water column became more stable (on Mar 11).

We can conclude that how the water temperature and salinity profiles change synchronously during late freezing and initial melting determines whether the under-ice convection takes place. Especially, if the sediment temperature is high and the transmitted radiation is large during freezing, the sediment and bottom water temperature can be warm and increase rapidly, increasing the probability for full-depth convection such as in winters of 2016 and 2018.

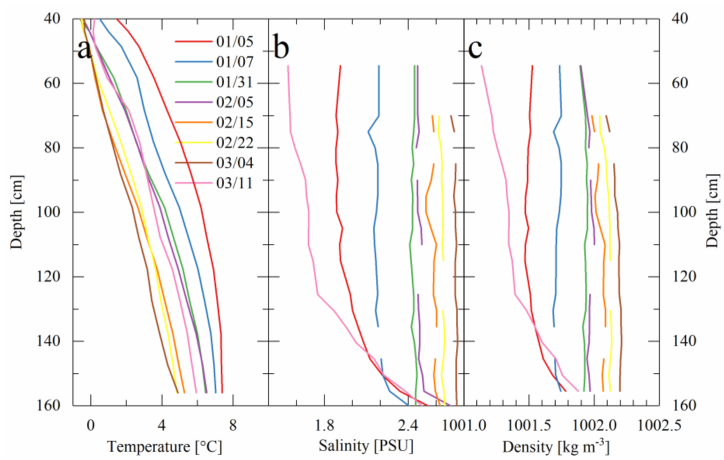

Figure 5. Observed temperature and salinity profiles and estimated water density (according to Leppäranta (2015)) in winter 2017.

3.3 Heat budget at the ice-water interface

Heat and mass fluxes at the ice-water interface govern the basal freezing/melting rates of ice cover and temperature of the top water layer. In mid-winter, the ice growth slowed down and then came to an equilibrium period (i.e. the thickness kept roughly constant) prior to the melting start (Fig. 3), so the latent heat flux Q_l kept positive due to continuous ice growth and then fluctuated near zero level. After the ice began to melt from bottom, Q_l turned negative (Fig. 6). The conductive heat flux Q_c through the bottom ice kept positive, indicating upward heat transport. After the ice started fast melting, Q_c came to near zero since the ice cover turned into a (quasi-)isothermal state.

The water-to-ice heat flux F_w showed similar variation with Q_c. Physically, F_w is crucially determined by the inverse thermal gradient of the topmost interface layer. Thinner interface layer with higher thermal gradient in winters 2016 (40.8±11.7 W m^{-2}) and 2018 (44.9±9.4 W m^{-2}) created higher F_w than those in winters 2017 (21.4±12.3 W m^{-2}) and 2019 (30.2±9.0 W m^{-2}). Interestingly, the convective mixing process increased F_w by 33% in winter 2016 but decreased F_w by 26% in winter 2018, indicating complicated effect of convection.

During the ice growth, both latent heat due to freezing (Q_l) and conductive heat from water to ice (F_w)

https://doi.org/10.5194/tc-2021-349
Preprint. Discussion started: 18 November 2021

The Cryosphere
Discussions
Open Access

were transported to the ice interior (Q_c) (Eq. (3)). The Q_c is predominantly determined by the ice thickness and air temperature according to analytical methods (Leppäranta, 2015), so higher F_w means lower Q_l, namely, smaller growth rate of ice. Specifically, F_w took up > 65% of Q_c prior to the equilibrium stage (e.g. winters of 2016 and 2017) and > 90% in the equilibrium stage (e.g. winters of 2018 and 2019).

During initial ice melting, the heat transferred from water to ice (F_w) was largely conducted to the ice interior (Q_c) (70%–80%) and partly used to melt the basal ice (Q_l). But during fast melting, Q_c was negligible and F_w was almost totally used for basal ice melt.

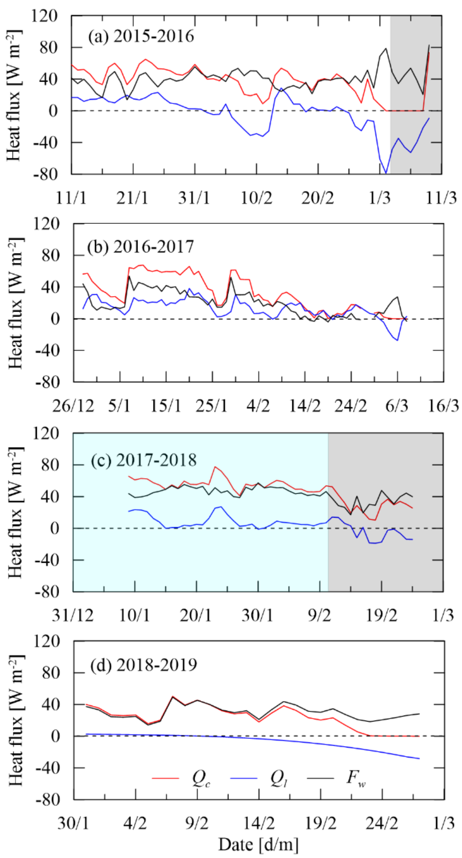

Figure 6. Heat fluxes at the ice-water interface (Q_c: conductive heat flux in the bottom ice; Q_l: latent heat flux due to basal ice freezing/melting; F_w: water-to-ice heat flux). The light gray and blue zones denote periods of convective mixing and stratification with local "warm" layer (Fig. 4), respectively.

3.4 Energetics of the water column

The temperature regime of under-ice water is governed by the heat budget. Fig. 7 showed all the heat fluxes involved and the balance residual. In mid-winters, R_w was 25–50 W m^{-2} under bare ice cover and drop to 1.5–13 W m^{-2} under ice with snow cover of varied thickness (1.5–8 cm) and age. Only 3%–14%

https://doi.org/10.5194/tc-2021-349
Preprint. Discussion started: 18 November 2021

(1–5 W m^{-2}) of R_w (i.e. R_{sed}) reached and directly heated the sediment surface (Fig. 3), which in turn released heat (F_{sed}) to the overlying water in mid-winters (1–3 W m^{-2}). F_w also showed annual and seasonal variations (10–60 W m^{-2}) and was generally smaller under snow-covered ice than that under bare ice, likely indicating the effect of transmitted irradiance. The heat content change (F_{Tw}) was typically small (–5–4 W m^{-2}) during freezing but grew up to 4–15 W m^{-2} during the initial melting. Evidently, the transmitted solar radiation (R_w) and water-to-ice heat transfer (F_w) dominated the heat balance of the under-ice water. Combining the 4-winter observations, the R_w was the largest heat source (34.8±18 W m^{-2}) and accounted for (92±9)% of the total source (R_w+F_{sed}) to the under-ice water, while F_w was the largest heat sink (34.3±15 W m^{-2}) and accounted for (96±38)% of the total sink (F_w + R_{sed} + F_{Tw}). The term (F_{sed} – R_{sed}) was only –0.8±2.7 W m^{-2} and F_{Tw} was 0.7±8.7 W m^{-2}, both of which can be neglected compared to others. Therefore, the transmitted solar radiation was almost totally (98%) returned to the ice base by means of water-to-ice heat conduction.

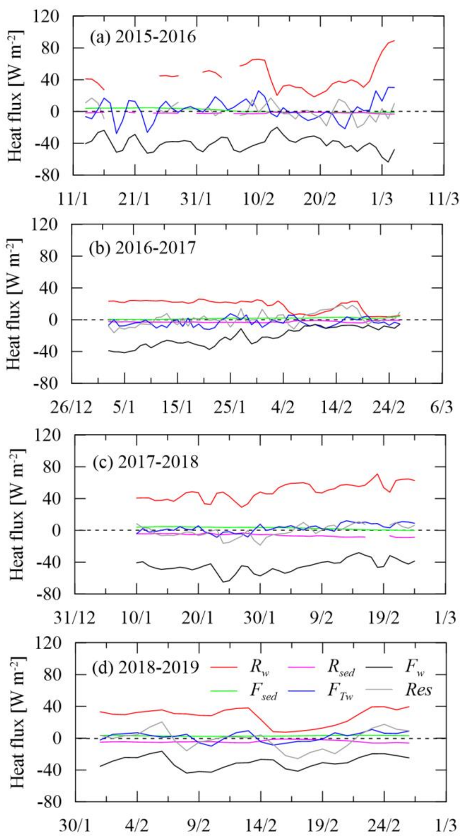

Figure 7. Heat budget of the under-ice water (R_w: transmitted solar radiation; Rsed: absorbed solar radiation by sediment; F_w: water-to-ice heat flux; F_{sed}: heat released from sediment; F_{Tw}: sensible heat caused by water heat content change; *Res*: residual of heat balancing, which is supposed to be zero when all heat fluxes balance ideally)

4 Discussion

4.1 Comparisons with (sub)Arctic and temperate climate lakes

Prior to the ice-on date, in freshwater lakes fall mixing due to thermally free convection (at 3.98°C) and continuous wind stirring usually creates large/full-depth vertical isothermal structure with temperature quite close to the freezing point (stage **I** in Fig. 8).

After the freeze-up or ice-on, the stratification evolves as a joint result of snow and ice condition, solar radiation penetration, bottom sediment heating, and horizontal current/circulation. In Arctic, boreal, and northern temperate regions, such as Fennoscandia, north American, and central Europe, winter precipitation leads to thick snow covers over the lake ice after the freeze-up, and little light can penetrate through the snow and ice covers, hence, the solar radiation input can be neglected within the water column. The water column only gets heat from the bottom sediment and releases heat to the top ice cover. Both heat fluxes are very small (0–5 W m^{-2}). Therefore, the lake water stays close to the freezing point and even presents a very weak inverse structure similar to curve **I** through the entire growth period (3–5 months). After the melting onset, warm air and strengthened solar radiation leads to snow melting, more solar radiation goes through the transparent ice and heats up the underlying water, creating a deepening convective mixing (stage **II**) before reaching the temperature of maximum density (T_m) (stage **III**). Usually, the ice cover breaks up before the thermal state of stage **III** forms in most deep boreal and Arctic lakes (Yang et al., 2020).

In mid-latitude cold and arid regions, intensive solar radiation and little snow allow more solar energy transmitting to the water column just following the freeze-up. In the Qinghai-Tibet Plateau (QTP), the water column can keep stably the state of stage **I** or starts slowly warming (i.e. period of stage **II**) just following the freeze-up in deep lakes, and then go to stage **III**, creating mid-winter overturn (Fig. 8b). Afterwards, stronger solar radiation due to thinner ice warms continuously the top water layer (stage **IV**), which exists for 4-6 weeks before breakup (Kirillin et al., 2021; Lazhu et al., 2021). However, in shallow ponds, stage **II** (i.e. transition from stage **I** to **III**) is very short-lived (one week), the water column roughly stays at stage **III** almost over the entire freezing period. And the following warm layer (**IV**) can deepen to near the lake bottom before ice-off (Fig. 8c) (Huang et al., 2019b).

Despite the intensive solar transmission, Lake Ulansuhai is very shallow and weak saline, its thermal stratification dynamics is determined by the synchronous profile evolution of temperature and salinity. Although our observation covered only the mid-winters, thermal profile of type **I** is expected at the pre-winter and ice-on due to joint effects of wind-stirring and large salinity gradient. But stage **I** should be very short and the bulk temperature increases rapidly and transits to stage **II** due to the strong solar transmission and small lake depth. The occurrence of stage **III** is conditional and mainly dependent upon the salinity change due to freezing-exclusion effect. Stage **IV** is also expected since meltwater dilution in the top layer can suppress the convection.

Salinity structure plays a more important role in lake stratification and convective mixing than temperature in saline and even freshwater lakes (Kirillin and Terzhevik, 2011). The present results indicated that the salt exclusion during freezing changes both the total salt content and salinity structure. For instance, for a lake with mean depth of 1.0 m, if the separation coefficient is assumed 0.15 (Pieters and Lawrence, 2009; Bluteau et al, 2017), formation of 0.5 m ice cover can cause an increment of 70% to the water salinity. In Lake Ulansuhai, the salinity increases downwardly at the ice-on with a large salinity gradient. Afterwards, as the ice grows, salt exclusion gradually decreases the salinity gradient, making the water more prone to mix convectively.

https://doi.org/10.5194/tc-2021-349
Preprint. Discussion started: 18 November 2021

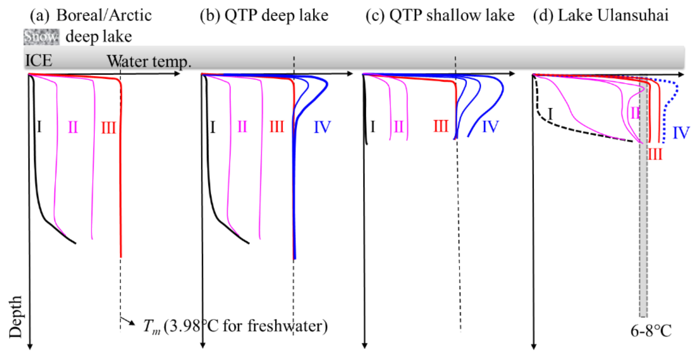

Figure 8. Typical thermal stratification types in ice-covered lakes: (a) deep lake in Arctic (Jakkila et al., 2009), (b) deep lakes in QTP (Kirillin et al., 2021; Lazhu et al., 2021), (c) a shallow pond in QTP (Huang et al., 2019b), and (d) Lake Ulansuhai. The definitions of Roman numbers are presented in the text.

4.2 What leads to high water-to-ice heat flux?

The water-to-ice heat flux F_w plays a predominant role in the basal growth and melting of lake ice cover, but is quite challenging to be observed instrumentally. Eqs. (1) and (3) provide two ways to calculate F_w if the ice thickness, temperature profiles of the ice-water-sediment column, and solar irradiation are observed (actually these variables are routinely observed).

By definition, F_w is the conductive heat across the very thin diffusive water layer just beneath the ice. Temperature difference and thickness (i.e. thermal gradient) of this thin layer are influenced to varied extent by thermal stratification, convective mixing (Figs. 4 and 5), advection due to horizontal currents and circulation (Rizk et al., 2014; Kirillin et al., 2015), and seiche oscillation (Kirillin et al., 2018). All of these thermal and hydraulic dynamic processes lead to Fw's nature of non-stationary and spatiotemporal variation (Winters et al., 2019).

In boreal and Arctic lakes, low solar radiation, short insolation duration, and most importantly thick snow cover limit solar heat input to the under-ice water column, just water and sediment heat release (both at very small flux) can cause only a low seasonal F_w (0–15 W m^{-2}) (Malm et al., 1997; Jakkila et al., 2009). However, in arid or mid-latitude lakes with little snow and/or more intensive solar insolation, F_w can be 10–50 W m^{-2} in Lake Baikal (Aslamov et al., 2017) and 20–100 W m^{-2} in QTP lakes, and shows distinct seasonal variation (Huang et al., 2019a,b; Kirillin et al., 2021). The estimated F_w in Lake Ulansuhai is comparable to Lake Baikal and QTP lakes, indicative of the vital contribution of solar radiation and the absence of snow cover.

From a perspective of heat balance in water (Eq. (1)),

$$F_w = R_w - R_{sed} + F_{sed} + F_h - \rho_w c_w h_w \frac{dT_w}{dt} - \rho_w c_w T_w \frac{dh_w}{dt}, \qquad (4)$$

If we define $Q_{rad} = R_w - R_{sed}$ (i.e., solar absorption by water column), and the heat content change due to subsurface water seepage is negligible,

Eq. (4) is transformed to

$$F_w = Q_{rad} + F_{sed} + F_h - F_{Tw}, \qquad (5)$$

which means the penetrated solar energy (Q_{rad}) and sediment heat (F_{sed}) are used to change the bulk water temperature (F_{Tw}) and its structure. In turn, the water body loses heat to the ice by adjusting its

https://doi.org/10.5194/tc-2021-349
Preprint. Discussion started: 18 November 2021

bulk temperature and structure. Fig. 7 argued that both F_{sed} and F_{Tw} are very small and roughly constant and Q_{rad} and F_w are the overwhelming dominator in heat source and sink, respectively. Therefore, Eq. (5) can be transformed to a linear formula to present the contribution of Q_{rad},

$$F_w = aQ_{rad} + b, \quad (6)$$

where the slope a and intercept b reflect the contributions of penetrated solar radiation and of sediment and advection heat, respectively. During our observations, a and b is 0.52 and 15.8 W m^{-2}, respectively, in Lake Ulansuhai (Fig. 9). This significant correlation also indicates directly the penetrated solar radiation is the first-order driver of seasonal and annual variations in water-to-ice heat transfer (Fig. 7). But we have to note that values of both coefficients should be lake-specific. For instance, lake depth and salinity modify the changes in convective mixing depth, bulk water temperature, and temperature structure caused by solar irradiance (Lazhu et al., 2021), and thus alter the relative contributions of solar radiation to water heat content and to heat transfer from water to ice.

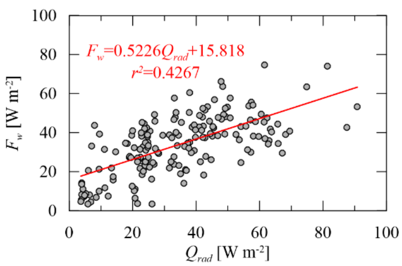

Figure 9. Linear fitting of daily water-to-ice heat flux F_w as a function of penetrated solar radiation Q_{rad}.

5 Conclusions

We present the ice-covered lake thermodynamics in a climatic and hydrological environment in distinct contrast to Arctic, boreal, and other northern temperate regions. The ice cover is always bare or only sparsely covered by occasional thin snow lasting for 1–2 weeks due to the arid climate. The clear ice cover allows 1/5–1/3 of incident solar radiation to penetrate into the water column in mid-winter, providing a background for energetics of under-ice water. The transmitted radiation and heat transfer across the ice-water interface dominate the heat budget of the water column and are highly correlated. High water-to-ice heat flux was observed and predominantly originated from the high irradiance. Both bulk water temperature and thermal structure are in quick response to transmitted radiation and snow events due to the small lake depth. Under-ice convective mixing takes place in certain winters and is dependent on both radiation and salinity profile, which is mediated by the salt exclusion during freezing. Salt exclusion effect (or cryoconcentration) on lake stratification and convection in shallow ice-covered freshwater and saline lakes needs to be investigated in future effort.

Data availability. The main datasets on lake ice/snow thickness, temperatures and transmitted solar radiation used in this paper are available at https://zenodo.org/record/4291840 (doi: 10.5281/zenodo.4291840).

Author contributions. WH, ML, and ZLi conceived the study. WZ, HY and ZLin conducted the field observations. WZ, CZ, RL and ZLi analysed data on meteorology and ice/snow conditions. WH and ML developed and ran the model. WZ, RL and WH calculated the heat budgets for the water column.

WH and WZ wrote the paper with contributions from all of the co-authors.

Competing interests. The authors declare no competing interests.

Acknowledgements. This study was funded by the National Key Research and Development Program of China (2019YFE0197600), National Natural Science Foundation of China (51979024), the Open Fund of State Key Laboratory of Frozen Soil Engineering (SKLFSE201813), the Program of Introducing Talents of Discipline to Universities (B08039), and the Fundamental Research Funds for the Central Universities (CHD) (300102291507). We are grateful to technicians of the National Ecologic Station in Lake Ulansuhai and the rest of our field team for their invaluable help in field campaigns.

References

Aslamov, I.A., Kozlov, V.V., Kirillin, G.B., Mizandrontsev, I.B., Kucher, K.M., Makarov, M.M., and Granin, N.G.: A study of heat transport at the ice base and structure of the under-ice water layer in southern Baikal, Water Resour. 44(3), 428–441, 2017.

Bernhardt, J., Engelhardt, C., Kirillin, G., and Matschullat, J.: Lake ice phenology in Berlin-Brandenburg from 1947–2007: observations and model hindcasts, Climatic Change, 112, 791–817, 2012.

Bluteau, C. E., Pieters, R., Lawrence, G. A., The effects of salt exclusion during ice formation on circulation in lakes, Environ. Fluid Mech., 17, 579-590, 2017.

Bouffard, D., Zdorovennova, G., Bogdanov, S., Efremova, T., Lavanchy, L., Palshin, N., Terzhevik, A., Vinnå, L. R., Volkov, S., Wüest, A., Zdorovennov, R., and Ulloa, H. N.: Under-ice convection dynamics in a boreal lake, Inland Waters, doi: 10.1080/20442041.2018.1533356, 2019.

Cavaliere E., and Baulch, H. M.: Denitrification under lake ice. Biogeochemistry, 137(3), 285-295, 2018.

Franz, D., Mammarella, I., Boike, J., Kirillin, G., Vesala, T., Bornemann, N., Larmanou, E., Lang, M., and Sachs, T.: Lake-atmosphere heat flux dynamics of a thermokarst lake in arctic Siberia, J. Geophys. Res.: Atmos., 123, 5222–5239. https://doi.org/10.1029/2017JD027751, 2018.

Griffiths, K., Michelutti, N., Sugar, M., Douglas, M. S. V., and Smol, J. P.: Ice-cover is the principal driver of ecological change in High Arctic lakes and ponds, PLoS ONE, 12(3), e0172989. doi:10.1371/journal.pone.0172989, 2017.

Huang, W., Cheng, B., Zhang, J., Zhang, Z., Vihma, T., Li, Z., and Niu, F.: Modeling experiments on seasonal lake ice mass and energy balance in the Qinghai-Tibet Plateau: a case study, Hydrol. Earth Syst. Sci. 23, 2173-3186, 2019a.

Huang, W., Zhang, J., Leppäranta, M., Li, Z., Cheng, B., and Lin, Z.: Thermal structure and water-ice heat transfer in a shallow ice-covered thermokarst lake in central Qinghai-Tibet Plateau, J. Hydrol., 578, 124122, doi: 10.1019/j.jhydrol.2019.124122, 2019b.

Huang, W., Zhang, Z., Li, Z., Leppäranta, M., Arvola, A., Song, S., Huotari, J., and Lin, Z.: Under-ice dissolved oxygen and metabolism dynamics in a shallow lake: The critical role of ice and snow, Water Resour. Res., 57, e2020WR027990, doi: 10.1029/2020WR027990, 2021.

Jakkila, J., Leppäranta, M., Kawamura, T., Shirasawa, K., Salonen, K.: Radiation transfer and heat budget during the ice season in Lake Pääjärvi, Finland, Aquat. Ecol., 43, 681–692, 2009.

Karetnikov, S., Leppäranta, M., and Montonen, A.: A time series of over 100 years of ice seasons on Lake Ladoga, J. Great Lakes Res., 43, 979–988, 2017.

Kirillin, G., Aslamov, I., Leppäranta, M., Lindgren, E.: Turbulent mixing and heat fluxes under lake ice: the role of seiche oscillations, Hydrol. Earth Syst. Sci., 22, 6493–6504, doi:10.5194/hess-22-6493-2018, 2018..

https://doi.org/10.5194/tc-2021-349
Preprint. Discussion started: 18 November 2021

Kirillin, G.B., Forrest, A.L. Graves, K.E., Fischer, A., Engelhardt, C., and Laval, B.E.: Axisymmetric circulation driven by marginal heating in ice-covered lakes, Geophys. Res. Lett., 42, 2893–2900, 2015.

Kirillin, G., Leppäranta, M., Terzhevik, A., Granin, N., Bernhardt, J., Engelhardt, C., Efremova, T., Golosov, S., Palshin, N., Sherstyankin, P., Zdorovennova, G., and Zdorovennov, R.: Physics of seasonally ice-covered lakes: a review, Aquat. Sci., 74, 659–682, 2012.

Kirillin, G., Shatwell, T., and Wen, L.: Ice-covered lakes of Tibetan plateau as solar heat collectors, Geophys, Res. Lett., 48, e2021GL093429, 2021.

Kirillin, G., Terzhevik, A.: Thermal instability in freshwater lakes under ice: Effect of salt gradients or solar radiation?, Cold Reg. Sci. Technol. 65(2), 184-190, 2011.

Lazhu, Yang, K., Hou, J., Wang, J., Lei, Y., Zhu, L., Chen, Y., Wang, M., and He, X.: A new finding on the prevalence of rapid water warming during lake ice melting on the Tibetan Plateau, Science Bulletin, https://doi.org/10.1016/j.scib.2021.07.022, 2021.

Leppäranta, M.: Freezing of lakes and the evolution of their ice cover, Springer, Berlin, Heidelberg, 2015.

Leppäranta, M., Lindgren, E., Wen, L., and Kirillin, G.: Ice cover decay and heat balance in Lake Kilpisjärvi in Arctic tundra, J. Limnol., 78, doi:10.4081/jlimnol.2019.1879, 2019.

Lei, R., Leppäranta, M., Cheng, B., Heil, P., and Li, Z.: Changes in ice-season characteristics of a European Arctic lake from 1964 to 2008, Climatic Change, 115(3-4), 725-739, 2012.

Lu, P., Cao, X., Li, G., Huang, W., Leppäranta, M., Arvola, L., Huotari, J., and Li, Z.: Mass and heat balance of a lake ice cover in the central Asian arid climate zone, Water, 12, 2888, doi:10.3390/w12102888, 2020.

Malm, J., Terzhevik, A., Bengtsson, L., Bovarinov, P., Glinsky, A., Palshin, N., and Petrov, M.: Temperature and salt content regimes in three shallow ice-covered lakes 2. Heat and mass fluxes, Hydrol. Res. 28, 129–152, 1997.

Pieters, R., Lawrence, G. A.: Effect of salt exclusion from lake ice on seasonal circulation, Limnol. Oceanogr., 54(2), 401-412, 2009.

Ptak, M., Sojka, M., and Nowak, B.: Effect of climate warming on a change in the thermal and ice conditions in the largest lake in Poland-Lake Śniardwy, J. Hydrol. Hydromech., 68(3), 260-270, 2020.

Rizk, W., Kirillin, G., and Leppäranta, M.: Basin-scale circulation and heat fluxes in ice-covered lakes, Limnol. Oceanol., 59(2), 445–464, 2014.

Shi, L., Li, Z., Niu, F., Huang, W., Lu, P., Feng, E., Han, H.: Thermal diffusivity of thermokarst lake ice in Beiluhe basin of the Qinghai-Tibet Plateau, Ann. Glaciol., 55(66), 153-158, 2014.

Song, S., Li, C., Shi, X., Zhao, S., Tian, W., Li, Z., Bai, Y., Cao, X., Wang, Q., Huotari, J., Tulonen, T., Uusheimo, S., Leppäranta, M., Loehr, J., and Arvola, L.: Under-ice metabolism in a shallow lake in a cold and arid climate, Freshwater Biol., http://doi.org/10.1111/fwb.13363, 2019.

Sun, B., Li, C. Y., Cordovil, C. M. D. S., Jia, K. L., Zhang, S., de Varennes, A., and Pereira, L. S.: Variability of water quality in Ulansuhai Lake receiving drainage water from Hetao Irrigation system in Yellow River Basin, China, Fresen. Environ. Bull., 22(6), 1666-1676, 2013.

Sun, B., Li, C. Y., and Zhu, D. N.: Changes of Ulansuhai Lake in past 150 years based on 3S technology, International Conference on Remote Sensing IEEE, doi:10.1109/rsete.2011.5964944, 2011.

Verpoorter, C., Kutser, T., Seekell, D. A., and Tranvik, L. J.: A global inventory of lakes based on high-resolution satellite imagery, Geophys. Res. Lett., 41(18), 6396-6402, 2014.

Volkov, S., Bogdaonv, S., Zdorovennov, R., Zdorovennova, G., Terzhevik, A., Palshin, N., Bouffard, D., and Kirillin, G.: Environ. Fluid Mech., 19, 751-764, 2019.

Wang, B., Ma, Y., Chen, X., Ma, W., Su, Z., and Menenti, M.: Observation and simulation of lake-air heat and water transfer processes in a high-altitude shallow lake on the Tibetan Plateau, J. Geophys. Res. Atmos., 120, 12

https://doi.org/10.5194/tc-2021-349
Preprint. Discussion started: 18 November 2021

327–12 344, 2015.

Winters, K. B., Ulloa, H. N., Wüest, A., and Bouffard, D.: Energetics of radiatively heated ice-covered lakes, Geohpys. Res. Lett., 45, 8913-8925, 2019.

Yang, B., Wells, M. G., McMeans, B. Dugan, H. A., Rusak, J. A., Weyhenmeyer, G. A.,Brentrup, J. A., Hrycik, A. R., Laas, A., Pilla, R. M., Austin, J. A., Blaunchfield, P. J., Carey, C. C., Guzzo, M. M., Lottig, N. R., Mackay, M. D., Middel, T. A., Pierson, D. C., Wang, J., and Young, J. D.: A new thermal categorization of ice-covered lakes, Geophysical Research Letters, doi: 10.1029/2020GL091374, 2020.

Yang, F., Cen, R., Feng, W., Zhu, Q., Leppäranta, M., Yang, Y., Wang, X., Liao, H.: Dynamic simulation of nutrient distribution in lakes during ice cover growth and ablation, Chemosphere, 281, 130781, https://doi.org/10.1016/j.chemosphere.2021.130781, 2021.

Yang, F., Li, C., Leppäranta, M., Shi, X., Zhao, S., and Zhang, C.: Notable increases in nutrient concentrations in a shallow lake during seasonal ice growth, Water Sci. Technol., 74(12), 2773-2883, 2016.

Zhu, D. N., Cathryn, R. M., Sun, B., and Li, C. Y.: The influence of irrigation and Ulansuhai Lake on groundwater quality in eastern Hetao Basin, Inner Mongolia, China, Hydrogeol. J., 22 (5), 1101-1114, 2014.